UCLA
UCLA Previously Published Works

Title
Correction to "Nanoalloying MgO–Deposited Pt Clusters with Si To Control the Selectivity of Alkane Dehydrogenation"

Permalink

Journal
ACS Catalysis, 9(5)

ISSN
2155-5435

Authors
Jimenez-Izal, Elisa
Zhai, Huanchen
Liu, Jiyuan
et al.

Publication Date
2019-05-03

DOI
10.1021/acscatal.9b01161

Peer reviewed

Nanoalloying MgO-Deposited Pt Clusters with Si for Controlling the Selectivity of Alkane Dehydrogenation

Elisa Jimenez-Izal,[a,b] Huanchen Zhai,[a] Jiyuan Liu,[a] Anastassia N. Alexandrova,[a,c,*]

[a] *Department of Chemistry and Biochemistry, University of California, Los Angeles, 607 Charles E. Young Drive, Los Angeles, California 90095-1569, United States*

[b] *Kimika Fakultatea, Euskal Herriko Unibertsitatea (UPV/EHU), and Donostia International Physics Center (DIPC), P. K. 1072, 20080 Donostia, Euskadi, Spain*

[c] *California NanoSystems Institute, Los Angeles, California, 90095, United States*

Corresponding Author E-mail: ana@chem.ucla.edu

ABSTRACT: Nanoalloying MgO-deposited Pt clusters with eight main-group elements was computationally screened for potential selectivity toward partial dehydrogenation of small alkanes. Si was revealed as a promising dopant for Pt across two clusters sizes, as it appears to favor stopping dehydrogenation of alkanes at alkenes. Pure Pt clusters on MgO(100) tend to strongly adsorb ethane and activate one of the C-H bonds, but then bind ethylene in the activated di-σ-fashion and even spontaneously dehydrogenate it. They also strongly bind C atoms, as the first step of deactivation by coking. PtSi clusters also bind and active ethane, but, in contrast to pure Pt clusters, bind ethylene preferentially in a weaker π-fashion and do not spontaneously dehydrogenate it. Additionally, the affinity of C atoms to PtSi is reduced by ca. 2 eV as compared to pure Pt clusters of the same size. Finally, Si stabilizes the clusters against dissociating single Pt atoms, and thus is predicted to slow down catalyst sintering by Ostwald ripening. Thus, Si is predicted to improve both selectivity and stability of Pt cluster catalysts. The cluster behavior appears to be linked to its spin

multiplicity: isomers with unpaired electrons exhibit high activity, and, while they are abundant for pure Pt clusters, Si tends to quench spins. Si also causes clusters to become more globular, with fewer valence-unsaturated Pt sites. The discovered properties of Si potentially exceed those of B, the recently proposed doping agent for Pt clusters whose effect on selectivity was confirmed experimentally (Ha, Baxer, Cass, Anderson, Alexandrova, J. Am. Chem. Soc. 2017, 139, 11568-11575).

1. INTRODUCTION

Surface-deposited metallic nanoclusters are interesting catalysts,[1-4] allowing to maximize the use of precious metals due to their high surface-to-volume ratio, and having specific catalytic activities that are highly sensitive to the atom- and electron-count.[5-7] Hence, catalytic properties of cluster-based catalysis are easily tunable through minor changes in the size and/or composition.[8-11] Pt clusters, for example, are catalytic toward dehydrogenation of light alkanes. Light alkenes, like propylene and ethylene, are the desirable products of this reaction, pivotal in industry, and used to produce a number of compounds, such as polymers or oxygenates.[12] The problem with the routine use of Pt clusters in catalysis is their rapid deactivation, which occurs mainly via two mechanisms: coking and sintering.[13,14] Undesirable deeper dehydrogenation can lead to carbon deposits on the catalyst surface that block the active sites, deactivating it. Suboptimal selectivity is a major problem for Pt-based commercial catalysts as well. In practice, catalyst regeneration is done by combustion of the coke at high temperatures. However, this regeneration process triggers deactivation via the second mechanism, sintering. Sintering or thermal deactivation is a common problem in all the metallic nanoclusters, due to their tendency to minimize their surface energy by agglomerating into bigger nanoparticles.

Different promoters have been explored to improve the durability of metallic catalysts. The most widely used dopant for Pt in alkane dehydrogenation is Sn. Tin induces geometric and electronic effects and, as a result, improves the selectivity of Pt, neutralizes the acidity of the support, and reduces metal sintering,[15-19] although Pt deactivation is still a major problem.[20] Other metals like Ga, In, and Zn have been also proposed as promoters for platinum.[21-24] Very recently we pointed to boron as additive to boost the catalytic performance of Pt nanoclusters supported on MgO(100).[25] Boration reduces the affinity of metallic nanoclusters to C and creates more sintering resistant catalysts. This first theoretical prediction led to a joint experimental and computational work,[26] where B was confirmed to improve the lifetime of $Pt_n/\alpha-Al_2O_3$, by reducing the affinity towards alkene, and thus minimizing the coke formation. Furthermore, no sintering was observed for the doped Pt_nB_m clusters. He^+ ion scattering, and CO temperature programmed desorption (TPD) were used to detect the number of available Pt sites on the cluster surface, before and after the cycles of catalytic dehydrogenation. While pure Pt clusters clearly lost their active sites via agglomeration into larger particles or site blocking by coke, borated clusters remain intact even after six cycles of dehydrogenation TPD.

Both B and Sn as useful dopants were discovered rather serendipitously, and it is therefore not impossible that other useful dopants exits, and there is an underlying common electronic structure rationale for their useful properties. In this work, we used small Pt clusters on MgO(100), to screen the main group elements as potential dopants or co-alloying agents that would increase the lifetime of Pt catalyst and improve the selectivity in ethane dehydrogenation. For the most promising dopant, Si, we investigated bigger clusters, in order to confirm the found benefits across cluster sizes.

2. METHODS

PW-DFT calculations were performed using the PBE[27] functional and PAW pseudopotentials,[28] as implemented in the Vienna Ab initio Simulation (VASP)

package.[29-32] All calculations were spin unrestricted. Bulk MgO was optimized using a plane wave cutoff energy of 520 eV and a dense Monkhorst–Pack 9 x 9 x 9 k-point grid, resulting in optimized lattice constant a = b = c = 4.209 Å. For triatomic Pt_3 and Pt_2X (X= Pt, B, N, Al, Si, P, S, Cl, Sn) clusters supported on MgO(100) a 3 x 3 x 3 unit cell was used, while a bigger 4 x 4 x 3 unit cell was used for Pt_7 and Pt_7Si, in order to avoid spurious interactions between the nearby images of the cluster. The bottom two layers of the support were kept fixed at the positions of the bulk. A vacuum separation of ca. 15 Å between repeating cells in z direction was added. The plane wave cutoff energy was set to 450 eV, and the convergence criteria for geometry (SCF) relaxation was set to 10^{-5} (10^{-6}). The 1 x 1 x 1 Γ-centered k-point grid was used for surface calculations.

For the triatomic Pt_2X clusters supported on MgO(100), the global minima were searched manually, using linear and triangular clusters as starting geometries, and depositing them in all the possible orientations on all possible binding sites. To search for the global minima of bigger clusters on MgO(100), and the most stable binding configurations of adsorbates on the clusters, we used several different techniques implemented in our in-house package, PGOpt package. First, the lowest-energy isomers of surface-deposited Pt_7 and Pt_7Si clusters were identified using the Basin-Hopping (BH) algorithm[33] adapted for surface-supported clusters. 10 structures, generated using second-order Bond Length Distribution Algorithm (BLDA)[34] were used as the starting point for BH. Within the framework of BH, the potential energy surfaces (PESs) of the surface-supported cluster was sampled at the temperature of 1500 K using Monte Carlo scheme. Secondly, to identify the most stable binding modes of ethylene and ethane on Pt_2X, Pt_7, and Pt_7Si, the low-energy bare cluster isomers were used as the reference states, upon which the sites of the ethylene and ethane binding were sampled. For each cluster isomer, we generated 50 structures with at least one cluster-molecule bond, and 20 structures with at least two cluster-molecule bonds. For the co-adsorption of two ethylene molecules on Pt_7 and Pt_7Si, and C_2H_3 + H on Pt_7Si

(for the transition state search of dehydrogenation of ethylene), we generated 50 structures with at least one cluster-molecule bond. The molecular rotation, the angle of approach, and the distance from the cluster surface were automatically sampled using BLDA approach.[34] For the electronic structure analysis, the Bloch states were calculated using the Quantum Espresso package.[35]

Transition state (TS) search was performed using the Climbing Image Nudged Elastic Band (CINEB). Clusters were mounted on a 3 layers MgO(100) surface slab. The convergence criterion for residual force was set to 0.02 eV•Å^{-1} for the TS calculation. All TS configurations were confirmed by phonon calculations, at Γ point.

3. RESULTS AND DISCUSSION

3.1 Pt$_2$X on MgO(100)

We considered the Pt$_2$X (X= Pt, B, N, Al, Si, P, S, Cl and Sn) clusters supported on MgO(100). Among these main group elements, Sn is a widely used promotor for Pt, and B was also recently proposed. Additionally, P, S and N are known to be poisons for Pt catalyst.[36,37] We included them in our pool for comparison. These elements were chosen because their supplies are larger and they would help reducing the price of the Pt catalysts. The identified most stable structures of Pt$_2$X on MgO(100) are shown in Figure 1. At first glance we see that the known poison atoms (S, P, and N) bind on top of Pt, avoiding the surface. This might be interpreted as these elements blocking the active sites. Chlorine adopts this position too. B, Sn, Si, and Al, however, prefer to interact directly with the surface oxygen atom. Note that the Pt$_3$ cluster has a different geometry from the structure reported in ref. 25, because of the more thorough search and tighter convergence settings used in the present study. The calculated Bader charges are indicative of charge transfer from the support to the Pt$_2$X clusters, the amount of which is similar for all X, and Pt is always negatively charged (except for Pt$_2$N). Details can be found in Table S1 and Figure S1 in the Supporting Information. The

charge distributions within the clusters, however, varies depending on the dopant. The more electronegative elements, N, S and Cl, withdraw some charge from Pt and are the only ones that have a negative charge. The rest of the dopants are positively charged, and the biggest positive charge is found for Si, Al and B; at the same time Pt exhibits the largest negative charge in these systems.
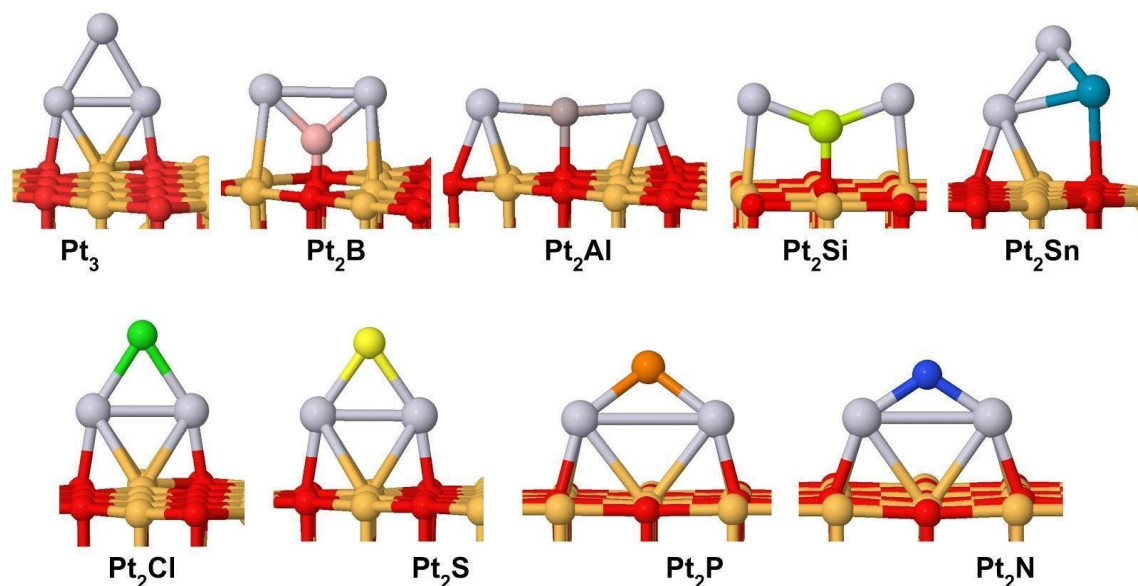

Figure 1. Calculated global minima of Pt_2X on MgO(100).

Next, we screen the small clusters for the affinity to a single C atom. Binding of one carbon atom can be considered as the first rudimentary event giving start to coke formation, which is a complex process, as we have successfully done in the past for predicting the tendency to undergo coke deposition.[25,26] In Figure 2 we show the most stable C-Pt_2X structures. Once again, the clusters doped with the poisons (P, S, N) are structurally differentiated, since C displaces these atoms and is located between them and Pt. Pt_2B, Pt_2Si, and Pt_2Al also have similar global minimum structures, where C binds to the farthest position from the dopant. C avoids Sn as well, but in this case C bonds to the surface oxygen, while Sn locates in the exterior of the cluster. The binding energies of C to the clusters are shown

Table 1. Notably, all the dopants except N, decrease the sticking energy to C compared to pure Pt. Cl, P and S have a less pronounced effect on the affinity to C. But B, Si, Sn, and Al show an outstanding impact on the affinity to C, reducing the binding energy by ~2 eV. Hence, these dopants so far show a promising trend in terms of potential catalytic selectivity.
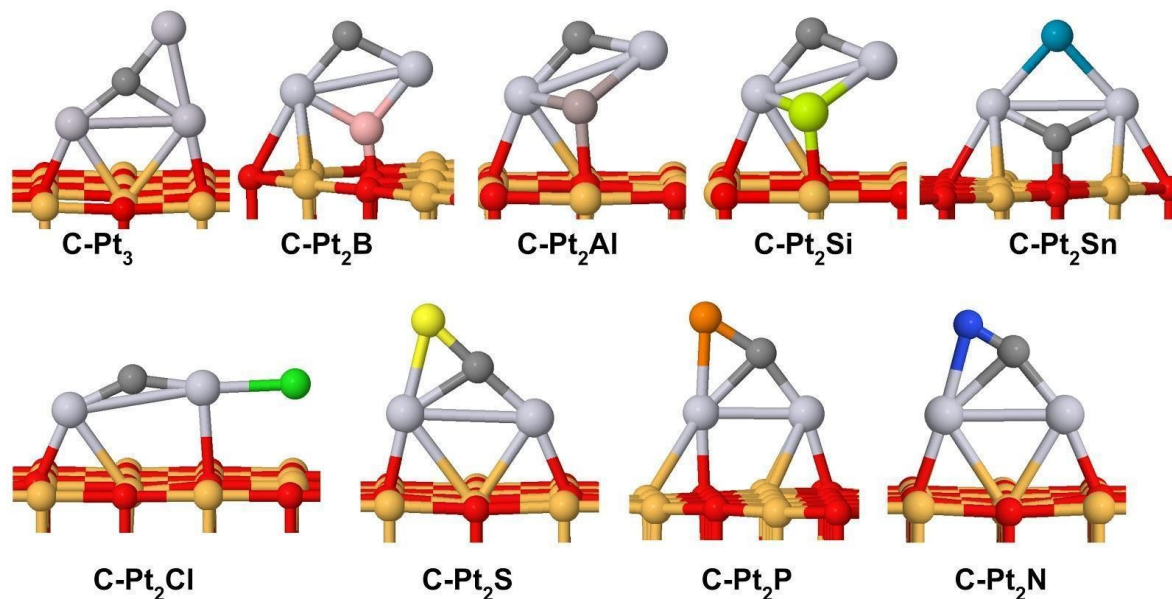

Figure 2. Putative global minima of C-Pt_2X.

The second major mechanism of deactivation of cluster catalysts is via sintering. For clusters under consideration sintering most often proceeds via Ostwald ripening,[14,38,39] i.e. dissociation of atoms from smaller clusters, migration, and association with larger clusters, although the particle migration and coalescence mechanism is also not to be discarded.[39] To account for the effect of dopants on the sintering propensities, we considered several energetic characteristics of our systems. The probability of particle migration and coalescence is dictated by the adsorption energy of the cluster to the surface:

(1) $E_{ads} = E(Pt_2X)_{supported} - E(surf) - E(Pt_2X)_{gas}$,

where $E(Pt_2X)_{supported}$ is the energy of the supported Pt_2X trimmer on MgO,

E(surf) is the energy of the pristine surface, and $E(Pt_2X)_{gas}$ the energy of the Pt_2X trimmer in gas phase. Thus, more strongly bound clusters are less likely to coalesce. In the Ostwald ripening regime, one atom is detached from the cluster and migrates through the surface, and the probability of this process is related to the energy penalty for one Pt atom to dissociate from the cluster:

$$(2)\ E_s = E(PtX)_{supported} + E(Pt)_{supported} - E(Pt_2X)_{supported} - E(surf)$$

where $E(PtX)_{supported}$ is the energy of the supported PtX dimer (i. e. after losing one Pt atom) on MgO, $E(Pt)_{supported}$ is the energy of a Pt atom supported on MgO, $E(Pt_2X)_{supported}$ stands for the energy of the supported Pt_2X trimmer on MgO, and E(surf) for the energy of the pristine MgO. The calculated E_{ads} and E_S are shown in Table 1. The pure Pt_3 cluster exhibits the largest adsorption energy, only comparable to Pt_2Cl. This might not be a big problem though, since Ostwald ripening is the prevalent sintering mechanism for small cluster size regime.[14] In line with this idea, we see that Pt_2Sn has the smallest E_{ads} of all clusters, but a larger penalty for dissociation of a Pt atom than Pt_3, while it is indeed known that Sn stabilizes Pt nanoparticles against sintering. Moreover, we recently showed that although Pt_7B/α-alumina has smaller E_{ads} than Pt_7/α-alumina, it has a higher dissociation penalty, and as a result - more resistant to deactivation, according to both theory and experiment.[11] Therefore, sintering energies are likely stronger indicators of the sintering tendency. Pure Pt clusters dissociate very easily, judging by the sintering energy, E_s, and E_s only worsen by introduction of Cl (Table 1). All other elements considered in this work improve the E_s energetic term; the most notable improvement is found for Pt_2B, followed by Pt_2P, Pt_2Al, and Pt_2Si. Note that all these elements seem to outperform Sn, a known stabilizer of Pt clusters against sitering.

Table 1. Energetic and electronic properties of Pt_2X deposited on MgO(100). Sintering energy E_s, adsorption energy E_{ads}, and binding energy to C BE[C] are given in eV. $\Delta Q_{cluster}$, ΔQ_{Pt}, and ΔQ_X are the total Bader charges on the cluster, on Pt and X atoms, respectively.

Cluster	E_s	E_{ads}	BE[C]	$\Delta Q_{cluster}$	ΔQ_{Pt}	ΔQ_X
Pt_3	-2.07	-4.18	-8.36	-0.58	-0.58	-
Pt_2B	-2.79	-3.88	-6.19	-0.21	-1.69	1.45
Pt_2Si	-2.30	-3.11	-6.09	-0.11	-2.22	2.12
Pt_2Sn	-2.13	-2.83	-6.22	-0.39	-1.09	0.69
Pt_2Al	-2.32	-3.81	-6.58	-0.41	-2.27	1.86
Pt_2Cl	-1.64	-4.09	-7.02	-0.59	-0.23	-0.36
Pt_2P	-2.46	-3.08	-7.02	-0.57	-0.96	0.40
Pt_2S	-2.02	-3.78	-7.52	-0.54	-0.33	-0.21
Pt_2N	-2.29	-3.47	-8.78	-0.58	0.02	-0.60

The results presented so far, taken together show that the most promising dopants are B and Sn (known promoters), as well as Al and Si (new). As mentioned before, Bader charges reveal that, while Pt is negatively charged in all the cases (except Pt_2N), the biggest negative charge on Pt is in

Pt$_2$Al, Pt$_2$Si, and Pt$_2$B. These results suggest that elements able to donate electrons to Pt have the potential to improve the coke- and sintering-resistances. This is one of the effects cited to explain the beneficial effects of alloying Pt with Sn on catalytic dehydrogenation. In the next section we will focus on the selectivity of the promising compositions, and we will see that a deeper look at the electronic structure is needed to properly explain the effect of various dopants.

3.2 Selectivity of Pt$_2$X for ethane dehydrogenation

To explore whether Si or Al might boost the selectivity of Pt catalysts, we calculated the adsorption of ethane and ethylene, the reactant and desirable product of partial dehydrogenation, respectively. Ideally, the catalysts would activate the reactant, while the product would desorb rather than dehydrogenate further. First, we calculated the most stable binding mode of ethane to Pt$_3$. As can be seen in Figure 3, in the most stable configuration, Pt activates a C-H bond, which is elongated from 1.11 Å to 1.18 Å. The configuration where ethane is just physisorbed (ethane-Pt$_3$ distance > 3 Å) is 0.19 eV less stable. Next, we looked for the most stable configuration of ethylene on Pt$_3$, and found that it spontaneously dehydrogenates ethylene. This result shows the extremely poor selectivity, that would give rise to a fast deactivation of the catalysts, and also brings to light one of the challenges of this reaction, which is the fact that the product is more reactive than the reactant. Can nanoalloying increase the catalyst lifetime? As concluded in the previous section, Al is one of the good candidates for alloying with Pt. Unfortunately the calculations of the adsorption of ethylene on Pt$_2$Al on MgO revealed that the system dehydrogenates ethylene as pure Pt does. Thus, Al does not improve the selectivity of dehydrogenation on deposited Pt clusters, and we stopped considering it at this point.
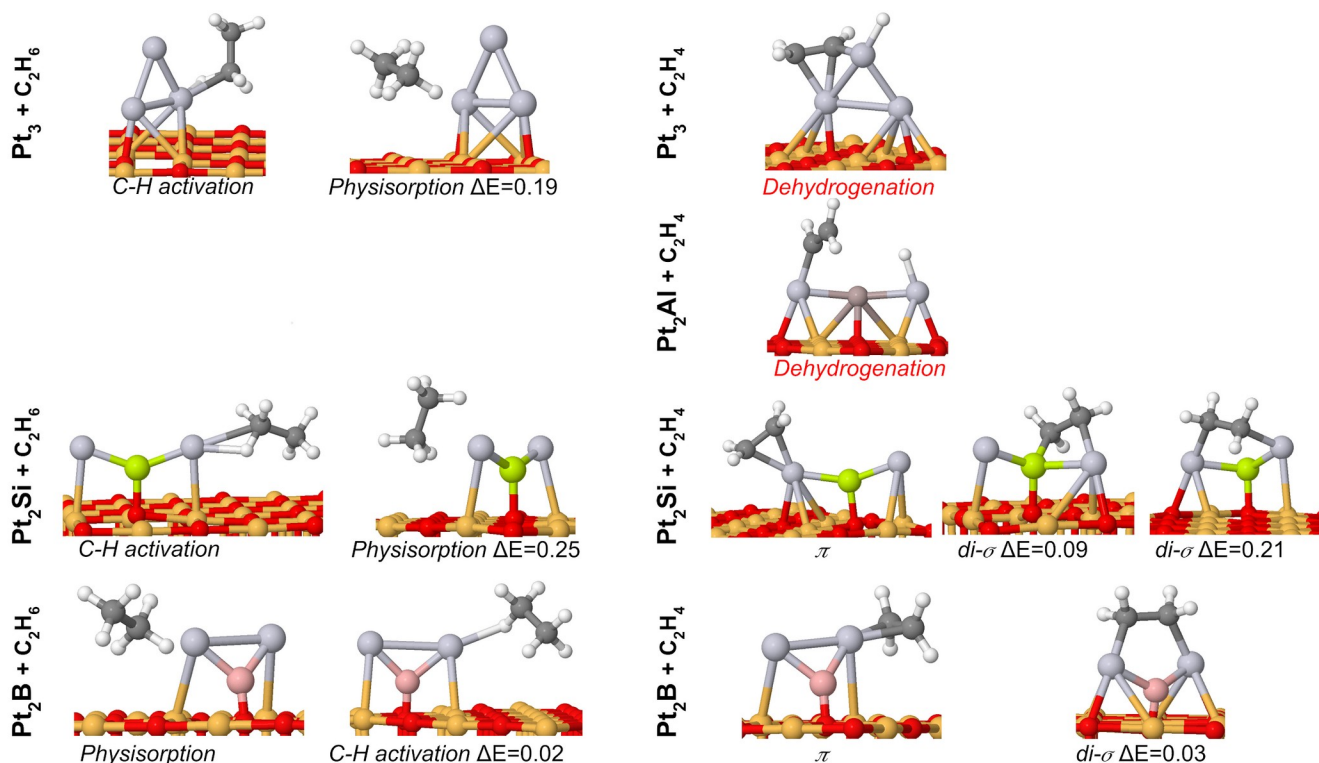
Figure 3. Most stable configurations of ethane and ethylene adsorbed on Pt$_2$X clusters. Energy differences are in eV. O, Mg, Pt, Si, B, C and H are depicted in red, orange, grey, yellow, pink, dark grey and white respectively.

However, for Pt$_2$Si on MgO, we found an encouraging scenario. On the one hand the C-H bond in ethane is activated, although the bond is elongated slightly less compared to pure Pt (to 1.13 Å). On the other hand, the ethylene binding is not suggestive of further dehydrogenation. Specifically, as it is well-established in the literature, ethylene binds to Pt either in di-σ or in π modes, and the former is considered a precursor of further dehydrogenation, whereas the latter is more likely to desorb.[41-44] For Pt$_2$Si, ethylene binds preferentially in the π mode. The di-σ binding to one Pt and Si atom is 0.09 eV less stable, and the di-σ mode to two Pt atoms is 0.21 eV less stable, suggesting that ethylene dehydrogenation is unlikely to follow. Importantly, no spontaneous dehydrogenation is observed for Si-doped Pt. We additionally calculated the reaction pathway for ethylene dehydrogenation starting from the Pt$_2$Si-ethylene di-σ structure, as shown in Figure 4. For the

dehydrogenated product, we search for the most stable $Pt_2Si + C_2H_3 + H$ structure (final product in Figure 4). The energy barrier for ethylene dehydrogenation is as high as 1.46 eV. Note that not only this barrier is high, but also in the case of pure Pt_3 the dehydrogenation is spontaneous, so the addition of Si shows a remarkable selectivity improvement, which will lead to an improved resistance to coke and a longer lifetime of the catalyst.
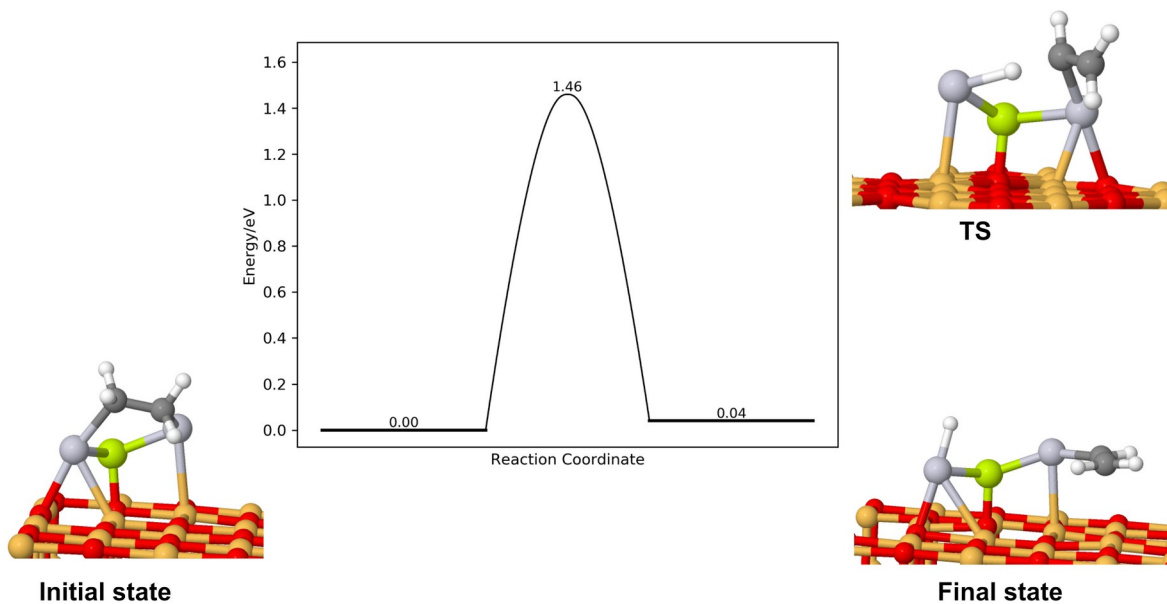

Figure 4. Reaction pathway for ethylene dehydrogenation on Pt_2Si. O, Mg, Pt, Si, C and H are depicted in red, orange, grey, yellow, dark grey and white respectively.

Finally and for comparison between the proposed dopant in the present study, Si, and the previously proposed dopant, B, we calculated the most stable binding modes for ethane and ethylene on Pt_2B. We see that this cluster behaves similar to Pt_2Si: it activates the C-H bond in ethane to the same extent as Pt_2Si (1.13 Å), and the π and di-σ binding modes of ethylene are almost degenerated. However, Si shows a slightly more adequate reactivity because i) the physisorption of ethane is less favored, while on Pt_2B it is energetically degenerated with the C-H bond activated geometry, and ii) regarding ethylene, the π interaction is slightly more energetically favored over di-σ than on Pt_2B. Therefore, we propose Si as a co-alloying

agent that would modulate the reactivity of Pt, making it more selective. Si was proposed as additive to Pd nanoparticles to improve the selectivity for hydrogenation of acetylene.[45-47] This correlates well with our results since the product of hydrogenating acetylene (C_2H_2) is ethylene (C_2H_4), the same product of dehydrogenating ethane.

Often the modified catalytic activity of clusters is attributed to charge transfer between the cluster and the support. However, here, the explanation based solely on the charge transfer would be unsatisfying. In fact, Pt has almost identical charge when alloyed with Al or Si. Indeed, the Projected Density of States, PDOS, (Figure S2) shows that in Pt_3 and Pt_2Al, the highest occupied Pt states (composed of d atomic orbitals) are at the edge of the valence band and they are located at very similar energies. The presence of aluminum does not change the location of states of Pt, indicative of metal-metal bonding in the nanoalloy. In the case of B-doped cluster, the highest occupied Pt states appear at lower energies, suggesting stabilizing covalent Pt-B interactions. In the Pt_2Si cluster, these Pt d-states are shifted to higher energies. Both B and Si thus must cause the misalignment of the Pt d-states with the antibonding electronic state of ethylene.

3.3 Structural characterization of Pt_7 and Pt_7Si

In the sub-nano cluster size regime, the properties change non-monotonically with the size. For this reason, it is possible that the projected beneficial effects of Si on the selectivity of Pt catalysts are specific to the smallest Pt_2Si (compared to Pt_3). For this reason we extended the study to Pt_7 and Pt_7Si on MgO(100). Pt_7 is an interesting size, where the peak of activity for ethylene dehydrogenation was seen,[11] and the effect of alloying with B on the catalyst lifetime was most remarkable of considered cluster sizes.[26]

The lowest-energy minima of Pt_7 on MgO(100) are shown in Figure 5, together with their Bader charges and Boltzmann populations at 700 K. A total of eight isomers lye within 0.40 eV and are predicted to be populated at this catalytically relevant temperature. At a first glance, there are two types

of isomers, and each of them constitutes approximately half of the population: cage-like isomers such as the putative global minimum (isomer I), and planar isomers that are perpendicular to the surface, like isomer II. The latter type is similar to Pt_5 on MgO(100),[48] which has a negative charge acquired from magnesia that leads to the flat geometry perpendicular to the surface. On α-alumina, Pt_7 also exhibits two types of geometries,[11] prismatic, like the global minimum, and single-layer ones that feature larger charge transfer from the support and are more reactive. In this case, however, the two types of Pt_7 isomers on MgO(100) exhibit similar charge transfer from the support (ca. 1.1 e[-]). However, there is an important difference between cage-like and planar isomers: while cage-like isomers have a closed-shell electronic structure, flat isomers have two unpaired electrons. As it turns out, this has an important impact on reactivity. Note that Isomers I and II have the highest Boltzmann population in the statistical ensemble of Pt_7 on MgO(100) (details of this calculation are given in the supporting information). Therefore, we focused on these two isomers for the reactivity analysis in the next section.

Then we investigated the effect of alloying with Si for this larger cluster, and focus on Pt_7Si on MgO(100) and its interaction with ethylene. It is possible that, depending on the method of eventual preparation, more Si atoms would integrate into the Pt cluster. However, as a first test, we consider just one Si atom, as we did also with B.[25,26] The predicted most stable Pt_7Si isomers are shown in Figure 6, together with their Bader charges and Boltzmann populations at 700K. As we observed in Pt_2Si, Si prefers to interact directly with the surface. Boron behaves similarly.[25,26,49] This is good, because the Pt sites are not blocked by the main group element. Compared to pure Pt clusters, more isomers are predicted to be populated in Si-doped clusters (12 vs 8) at 700 K. The isomeric diversity is an interesting phenomenon: because of isomers of different shapes, more diverse binding sites become available, an incoming adsorbate would be more likely to find a site of just the right affinity to undergo a reaction. The first six isomers of

Pt$_7$Si are cage-like, with Si at the center of the cluster and interacting directly with the surface oxygen. These isomers constitute the 87.8% of the population at 700 K. The rest of the structures are more diverse and generally more elongated. The total charge transfer from the support is in the range of 0.80 to 1.10 e$^-$. As in the smaller cluster, Si is positively charged (1.85-2.20 e$^-$), and Pt atoms have bigger negative charge than in pure Pt$_7$. All the conformers have a closed-shell electronic structure, except for two of them that possess two unpaired electrons. Unlike in pure Pt$_7$, the isomers with two unpaired electrons have also cage-like geometries. Notice the relatively high populations of Isomers B and C in the ensemble; those are due to the triplet spin states. In order to investigate the selectivity of Pt$_7$Si, in the next section we explored the reactivity of Pt$_7$Si focusing on three representative cluster isomers: the putative global minimum (Isomer A) and the two isomers with unpaired electrons (Isomers B and C).
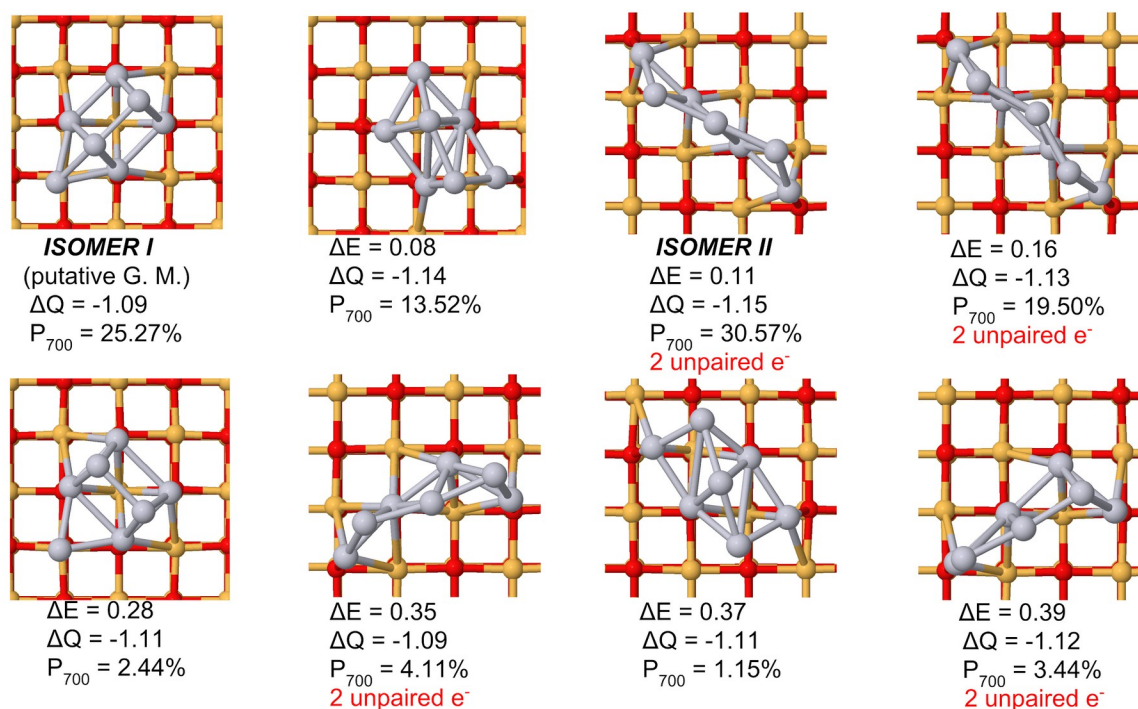

ISOMER I
(putative G. M.)
ΔQ = -1.09
P$_{700}$ = 25.27%

ΔE = 0.08
ΔQ = -1.14
P$_{700}$ = 13.52%

ISOMER II
ΔE = 0.11
ΔQ = -1.15
P$_{700}$ = 30.57%
2 unpaired e$^-$

ΔE = 0.16
ΔQ = -1.13
P$_{700}$ = 19.50%
2 unpaired e$^-$

ΔE = 0.28
ΔQ = -1.11
P$_{700}$ = 2.44%

ΔE = 0.35
ΔQ = -1.09
P$_{700}$ = 4.11%
2 unpaired e$^-$

ΔE = 0.37
ΔQ = -1.11
P$_{700}$ = 1.15%

ΔE = 0.39
ΔQ = -1.12
P$_{700}$ = 3.44%
2 unpaired e$^-$

Figure 5. Lowest-energy minima of Pt$_7$ on MgO(100), along with the energy difference of each isomer with respect to the putative global minima, ΔE, in eV. Charge transfer from the support to the whole cluster, ΔQ, and their Boltzmann populations at 700 K are shown.

For MgO the presence of oxygen vacancies is believed to be crucial for the catalytic activity.[50] Therefore, we additionally modeled the most relevant Pt_7 and Pt_7Si clusters mounted on the surface with an oxygen vacancy. Since global optimization search for this size clusters is intensely expensive, our approach has been to start from the minima structures on the stoichiometric MgO(100) surface, remove the oxygen atoms of the top MgO layer, and optimize all the resulting possible structures. Using this procedure, it is observed that the presence of O vacancy does not change the number of unpaired electrons and has a little effect on the geometry, as it can be seen in Figures S3 and S4. The most notable effect is that the charge transfer from the support is enlarged, but most of this charge is located on the atom that is directly bonded to the F-center and which is at the same time one of the least accessible for reactants. Due to the enhanced charge transfer, the binding energy of the cluster to the support is increased significantly. Thus, vacancies stabilize both Pt_7 and Pt_7Si clusters. The adsorption energy of Pt_7 and Pt_7Si to the stoichiometric MgO(100) is similar (unlike Pt_7B, that has smaller adsorption energy than Pt_7)[26], but the defected surface stabilizes the pure Pt clusters more. Thus, pure and Si doped Pt clusters will be more sintering resistant (at least via particle coalescence mechanism) on MgO surfaces containing F-centers. This is especially true for pure Pt clusters. Regarding the selectivity, F-centers do not change the relative stability between Pt_7Si isomers, but it has a profound effect on pure Pt catalysts: in the presence of O vacancies, the Pt_7 Isomer II (that will be shown to be least selective in the next section) becomes thermodynamically more stable than the Isomer I, and thus predominant in the population.
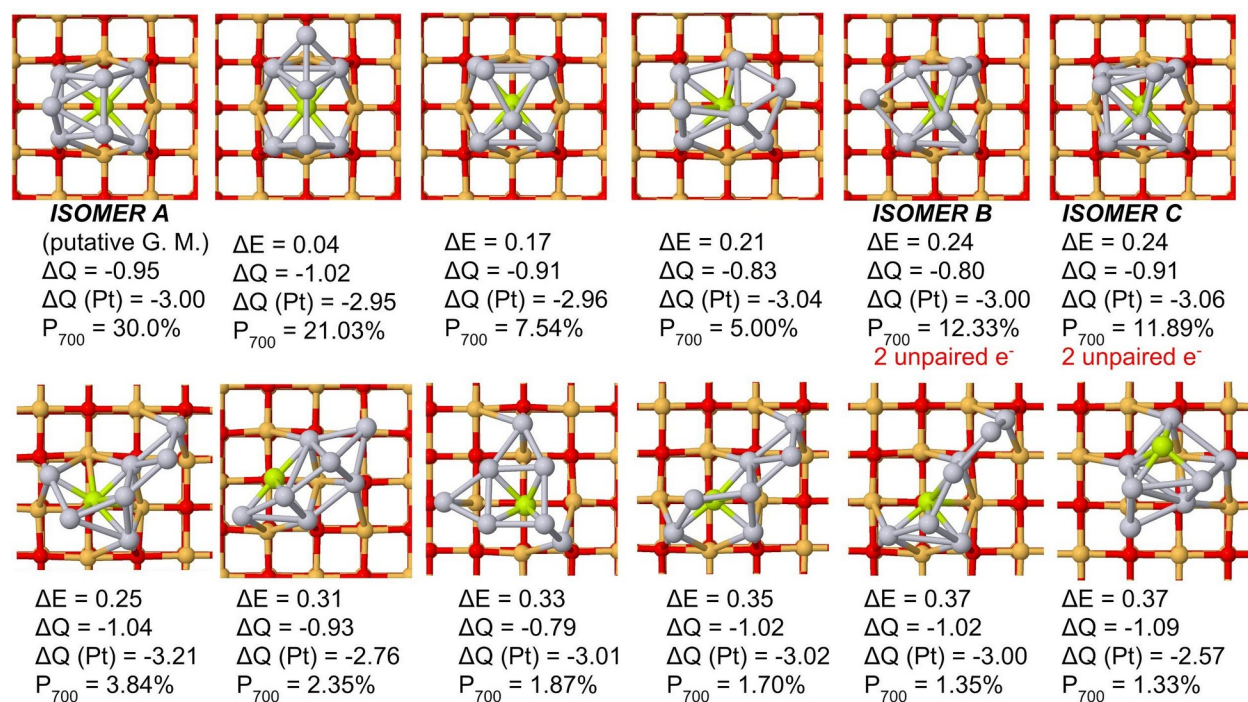
Figure 6. Lowest-energy minima of Pt_7Si on MgO(100), along with the energy difference of each isomer with respect to the putative global minima, ΔE, in eV. Charge transfer from the support to the whole Pt_7Si cluster, ΔQ, and Bader charges on the Pt atoms, $\Delta Q(Pt)$, and their Boltzmann populations at 700 K are shown. O, Mg, Pt and Si are depicted in red, orange, grey, and yellow respectively.

The values shown below each structure are:

Row 1:
- ISOMER A (putative G. M.), ΔQ = -0.95, ΔQ (Pt) = -3.00, P_{700} = 30.0%
- ΔE = 0.04, ΔQ = -1.02, ΔQ (Pt) = -2.95, P_{700} = 21.03%
- ΔE = 0.17, ΔQ = -0.91, ΔQ (Pt) = -2.96, P_{700} = 7.54%
- ΔE = 0.21, ΔQ = -0.83, ΔQ (Pt) = -3.04, P_{700} = 5.00%
- ISOMER B, ΔE = 0.24, ΔQ = -0.80, ΔQ (Pt) = -3.00, P_{700} = 12.33%, 2 unpaired e⁻
- ISOMER C, ΔE = 0.24, ΔQ = -0.91, ΔQ (Pt) = -3.06, P_{700} = 11.89%, 2 unpaired e⁻

Row 2:
- ΔE = 0.25, ΔQ = -1.04, ΔQ (Pt) = -3.21, P_{700} = 3.84%
- ΔE = 0.31, ΔQ = -0.93, ΔQ (Pt) = -2.76, P_{700} = 2.35%
- ΔE = 0.33, ΔQ = -0.79, ΔQ (Pt) = -3.01, P_{700} = 1.87%
- ΔE = 0.35, ΔQ = -1.02, ΔQ (Pt) = -3.02, P_{700} = 1.70%
- ΔE = 0.37, ΔQ = -1.02, ΔQ (Pt) = -3.00, P_{700} = 1.35%
- ΔE = 0.37, ΔQ = -1.09, ΔQ (Pt) = -2.57, P_{700} = 1.33%

3.4 Selectivity of Pt_7 vs Pt_7Si

We must emphasize the enormous computational cost of searching for the most stable isomers of these clusters made of 7 and 8 atoms deposited on a support, and the subsequent search of the most stable binding modes/sites of adsorbates on them. For this reason, in this section we did not look at the interaction of ethane with Pt_7 and Pt_7Si, but focused on the interaction with carbon, ethylene, as well as the co-adsorption two ethylene molecules, the most important species to account for the selectivity of the catalysts. In order to investigate the selectivity of Pt_7 and Pt_7Si, and taking

into account the high computational cost of these calculations, considered Isomers I and II of Pt_7 and Isomers A, B and C of Pt_7Si as representative.

First we calculated the most stable structures of carbon bonded to Pt_7 and Pt_7Si (Figure S5). For pure Pt_7, the binding energies to C are slightly smaller than for Pt_3, whereas for Pt_7Si these energies are larger than for Pt_2Si. Nevertheless Si still reduces the C sticking energies, and the strength of the effect might be dependent on the concentration of Si.

Then we calculated the most stable binding modes for ethylene on Pt_7 Isomers I and II (Figure 7). Ethylene binds to Isomer I preferentially in the π-fashion, the di-σ geometry being 0.27 eV less stable. Isomer II, however, binds ethylene in the di-σ fashion, but this is very close in energy to the dehydrogenated structure. Isomer II is therefore, more reactive than isomer I. Moreover, although Isomer I is more stable than Isomer II (by 0.11 eV), in the presence of ethylene Isomer II becomes more stable (by 0.19 eV). Taking into consideration not only the most stable isomer, but other thermally-accessible isomers, preferentially as a full ensemble, is essential for the correct description of the catalytic properties of these systems, as we have seen in the past as well.[9-11,26]

In order to consider the effect of the coverage on the selectivity of pure Pt nanocatalysts, we calculated the most stable binding sites on Isomer I and II, for two ethylene molecules adsorbed simultaneously (Figure S6). Overall the binding energies are slightly smaller than for a single adsorbate, and the reactivity of the two isomers (judged by the binding modes and their relative stabilities) gets closer: for Isomer II di-σ mode is stabilized with the coverage, and for Isomer II π adsorption mode is stabilized. For the latter we still find spontaneous dehydrogenation happening, but it is energetically less preferred as compared to dehydrogenation of a single ethylene molecule.
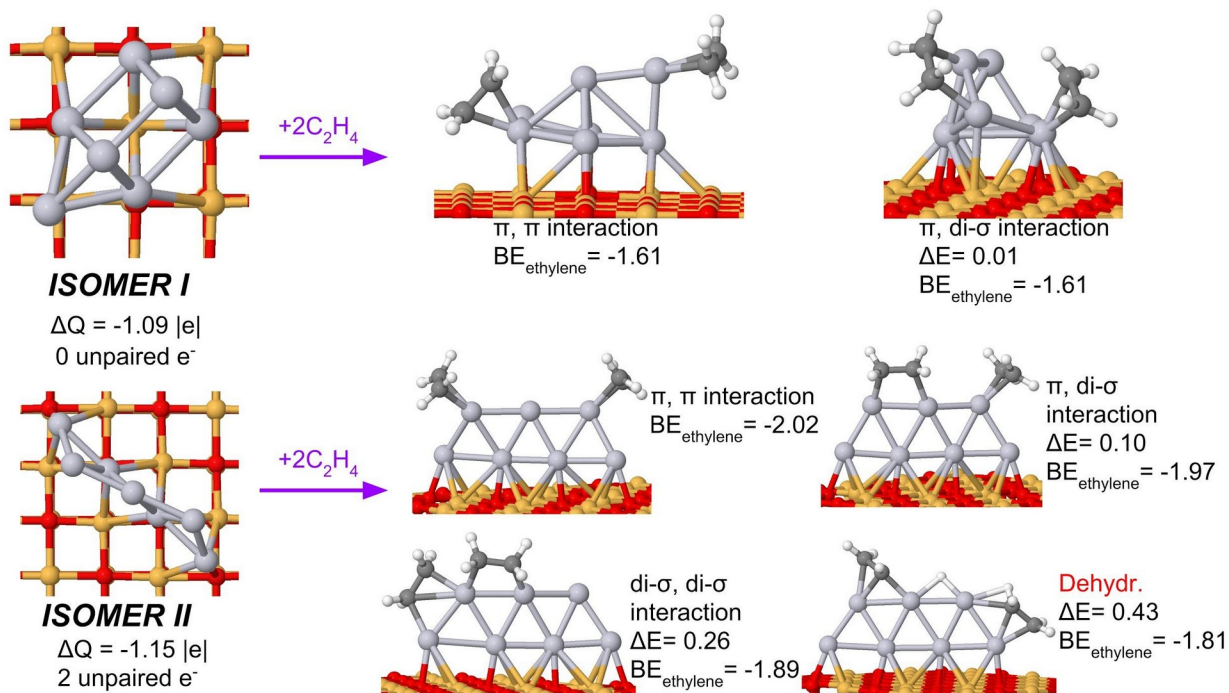
Figure 7. Most stable configurations of ethylene adsorbed on Isomers I and II of Pt$_7$ on MgO(100). Energy differences are given in eV. O, Mg, Pt, C and H are depicted in red, orange, grey, dark grey and white respectively.
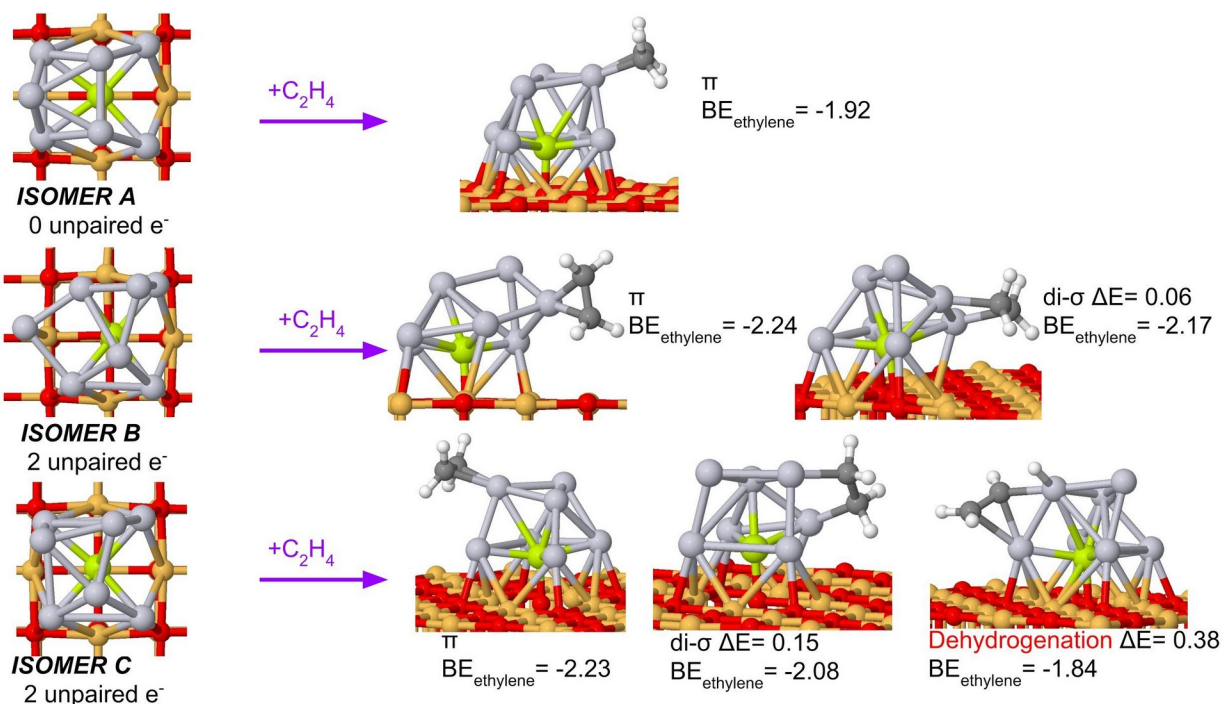
Figure 8. Most stable configurations of ethylene adsorbed on Pt$_7$Si Isomer A, B, and C. Energy differences are given in eV. O, Mg, Pt, Si, C and H are depicted in red, orange, grey, yellow, dark grey and white respectively.

Regarding Isomers A, B and C of Pt$_7$Si, the global minimum (Isomer A) is so selective that ethylene binds to it only in a π fashion (di-σ geometries are 0.40 eV higher in energy, i.e. unfeasible at typical temperatures of dehydrogenation), see Figure 8. For the isomers with unpaired electrons di-σ binding mode is more accessible, but still, the π geometry is preferred. Dehydrogenation is found only for Isomer C, and the resultant configuration is 0.38 eV less stable than the π interaction. Ethylene adsorption also alters the relative energy of the conformers; while Isomer A is 0.24 eV more stable than Isomers B and C, upon the adsorption of ethylene Isomer B becomes more stable (by 0.08 eV). We have additionally calculated the reaction pathway for ethylene dehydrogenation on the di-σ structure of the most reactive Isomer C, as shown in Figure 9. Two alternative reaction pathways are proposed, one in which the dissociated hydrogen is on top of the cluster, and the other one where it is at the bottom. The most favorable

configuration of the product on Pt_7Si is 0.40 eV more stable than Isomer C with the adsorbed intact ethylene (in the π configuration). Nevertheless, the appreciable barrier (0.61 eV) indicates that dehydrogenation does not happen spontaneously, as in the case of pure Pt_7. This barrier is smaller than on Pt_2Si, but note that on pure Pt_7 (Isomer II) the dehydrogenation is barrierless. Therefore, Si improves the selectivity of Pt by reducing its reactivity towards ethylene, improving in this way its resistance to products of deeper dehydrogenation, i.e. coke.
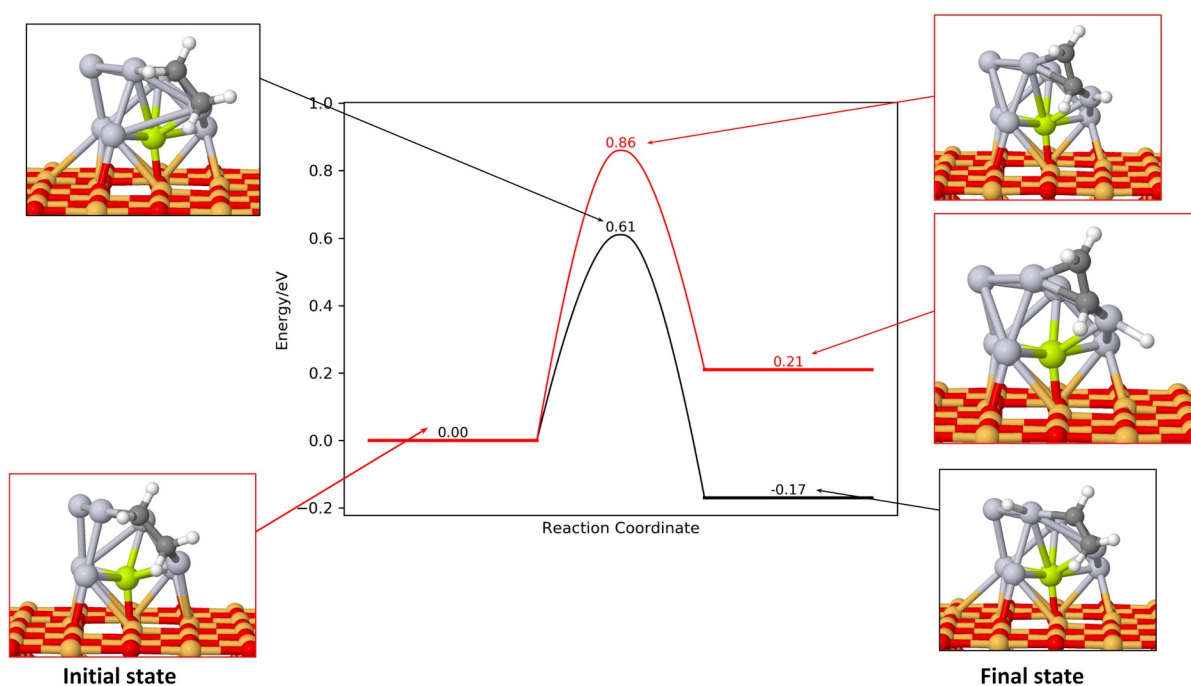
Figure 9. Reaction pathway for ethylene dehydrogenation on Pt_7Si. Two alternative reaction pathways are shown. O, Mg, Pt, Si, C and H are depicted in red, orange, grey, yellow, dark grey and white respectively.

Finally, we calculated the most stable binding modes of two ethylene molecules on silicate clusters (Figure S7). As in the case of pure Pt, co-adsorption slightly decreases the binding energies. The predicted selectivity is very similar for one or two ethylene molecules bound to the catalysts, i.e. di-σ and dehydrogenated structures are disfavored. The most remarkable

difference is that the dehydrogenation on Isomer C is energetically even less favorable at the higher coverage.

In order to understand the origin of the different reactivity between Isomers I and II, we analyzed their frontier molecular orbitals (MOs): the lowest unoccupied molecular orbital (LUMO), the highest occupied molecular orbital (HOMO), and the HOMO-1 of these systems (Figure S8). MOs of Isomer I have marginal contributions from the most exposed Pt atoms, i.e. the electron density is concentrated is the part of the cluster close to the support. Conversely, Isomer II shows important contributions of the most exposed Pt atoms to these frontier MOs. This picture explains why ethylene interacts more strongly with Isomer II, since for C-H bond cleavage, electronic density is back-donated to the LUMO of ethylene. Of course, most of the spin density of Isomer II is also located on the three Pt atoms that are the farthest from the support, making them most reactive (Figure 10). Regarding Pt_7Si, the spin density plot helps understanding the higher reactivity of Isomer C compared to Isomer B (see Figure 10): for the latter most of the spin density is located on the atoms bonded to the surface, whereas in the former the spin density is located on the most exposed Pt atoms that are ready to bind reactants. So, as we found with Pt_7, the Pt_7Si isomers with unpaired electrons are more reactive, and thus less selective. However, the reactivity is lower than that of Pt_7, and the ethylene dehydrogenation is predicted to be marginal. We can therefore conclude that Si boosts the selectivity of Pt nanocatalysts.
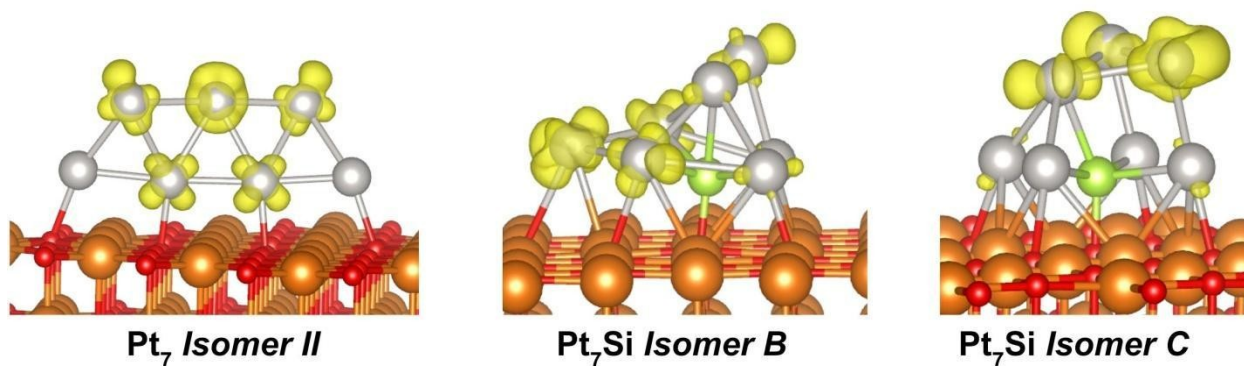

Figure 10. Spin density of Pt_7 Isomer II, and Pt_7Si Isomer B and C.

4. Conclusions

In this work we performed a computational screening of main group elements as potential co-alloying agents for surface-mounted Pt clusters, with the goal of manipulating the selectivity of catalytic dehydrogenation away from coking. We predicted a new promising dopant, Si, which stabilizes the clusters against Ostwald ripening, and discourages dehydrogenation of ethylene, as compared to pure Pt clusters. The effect is persistent across cluster sizes that we considered.

We find that silicon, just as boron,[25,26] modify the selectivity of platinum by inducing both electronic and geometric changes. We have shown cage-like isomers, as well as isomers with closed-shell electronic structure, tend to be less reactive and thus, more selective. Si induces electronic changes because, while for Pt_7 half of the population have unpaired electrons, for Pt_7Si this population represents less than 25 % of the isomers. At the same time, silicon clearly induces geometric effects of Pt clusters, since Si-doped clusters are more compact and spherical. Similar effect is produced by B on Pt_7 clusters supported on α-alumina.[11,26]

In most of industrial applications Pt is deposited on alumina, rather than magnesia. In the present work we modeled MgO-deposited clusters to alleviate the high computational cost, because both MgO and Al_2O_3 are simple non-reducible oxides with pronounced ionic character, and so the binding properties are expected to be similar.[1] In addition, our previous studies showed that the effect of using B as a dopant for MgO-supported Pt clusters is similar to that when such clusters as supported on alumina. Probably the biggest difference is that alumina is rougher, which is an advantage in terms of reducing the mobility and sintering of the clusters on the surface.

We emphasize that the results obtained in this work rely on the novel[9-11,26] paradigm of theory of cluster catalysis, where an ensemble of accessible

catalyst states is considered in property evaluations. Without accounting for alternative isomers thermally populated in conditions of catalysis, the presented effects would not be found.

ASSOCIATED CONTENT

Bader charges of Pt_2X putative global minima, PDOS of MgO(100) deposited Pt_3, Pt_2Al, Pt_2B, and Pt_2Si, effect of defects on the support as well as adsorbate coverage on Pt_7 and Pt_7Si, C binding to Pt_7 and Pt_7Si, and molecular orbitals of Pt_7 and Pt_7Si.

REFERENCES

(1) Kaden, W. E.; Wu, T.; Kunkel, W. A.; Anderson, S. L. Electronic Structure Controls Reactivity of Size-Selected Pd Clusters Adsorbed on TiO_2 Surfaces. *Science* **2009**, *326*, 826−829.

(2) Vajda, S.; Pellin, M. J.; Greeley, J. P.; Marshall, C. L.; Curtiss, L. A.; Ballentine, G. A.; Elam, J. W.; Catillon-Mucherie, S.; Redfern, P. C.; Mehmood, F.; Zapol, P. Subnanometre Platinum Clusters as Highly

Active and Selective Catalysts for the Oxidative Dehydrogenation of Propane. *Nat. Mater.* **2009**, *8*, 213−216.

(3) Lee, S.; Molina, L. M.; Lopez, M. J.; Alonso, J. A.; Hammer, B.; Lee, B.; Seifert, S.; Winans, R. E.; Elam, J. W.; Pellin, M. J.; Vajda, S. Selective Propene Epoxidation on Immobilized Au(6-10) Clusters: the Effect of Hydrogen and Water on Activity and Selectivity. *Angew. Chem., Int. Ed.* **2009**, 48, 1467−1471.

(4) Kwon, G.; Ferguson, G. A.; Heard, C. J.; Tyo, E. C.; Yin, C.; DeBartolo, J.; Seifert, S.; Winans, R. E.; Kropf, A. J.; Greeley, J.; Johnston, R. L.; Curtiss, L. A.; Pellin, M. J.; Vajda, S. Size-Dependent Subnanometer Pd Cluster (Pd_4, Pd_6, and Pd_{17}) Water Oxidation Electrocatalysis. *ACS Nano* **2013**, 7, 5808−5817.

(5) Lei, Y.; Mehmood, F.; Lee, S.; Greeley, J.; Lee, B.; Seifert, S.; Winans, R. E.; Elam, J. W.; Meyer, R. J.; Redfern, P. C.; Teschner, D.; Schlögl, R.; Pellin, M. J.; Curtiss, L. A.; Vajda, S. Increased Silver Activity for Direct Propylene Epoxidation via Subnanometer Size Effects. *Science* **2010**, 328, 224−228.

(6) Herzing, A. A.; Kiely, C. J.; Carley, A. F.; Landon, P.; Hutchings, G. J. Identification of Active Gold Nanoclusters on Iron Oxide Supports for CO Oxidation. *Science* **2008**, 321, 1331–1335.

(7) Watanabe, Y; Wu, X.; Hirata, H.; Isomura N. Size-dependent Catalytic Activity and Geometries of Size-Selected Pt Clusters on TiO_2(110) Surfaces. *Catal. Sci. Technol.* **2011**, 1, 1490–1495.

(8) Heiz, U.; Sanchez, A.; Abbet, S.; Schneider, W.-D. Catalytic Oxidation of Carbon Monoxide on Monodispersed Platinum Clusters: Each Atom Counts. *J. Am. Chem. Soc.* **1999**, 121, 3214−3217.

(9) Zhang, J.; Alexandrova, A. N. The Golden Crown: A Single Au Atom that Boosts the CO Oxidation Catalyzed by a Palladium Cluster on Titania Surfaces. *J. Phys. Chem. Lett.* **2013**, 4, 2250−2255.

(10)   Ha, M.-A.; Dadras, J.; Alexandrova, A. N. Rutile-Deposited Pt–Pd clusters: A Hypothesis Regarding the Stability at 50/50 Ratio. *ACS Catal.* **2014**, 4, 3570−3580.

(11)   Baxter, E. T.; Ha, M.-A.; Cass, A. C.; Alexandrova, A. N.; Anderson, S. L. Ethylene Dehydrogenation on $Pt_{4,7,8}$ Clusters on Al_2O_3: Strong Cluster Size Dependence Linked to Preferred Catalyst Morphologies. *ACS Catal.* **2017**, 7, 3322-3335.

(12)   Sattler, J. J. H. B.; Ruiz-Martinez, J.; Santillan-Jimenez, E.; Weckhuysen, B. M. Catalytic Dehydrogenation of Light Alkanes on Metals and Metal Oxides. *Chem. Rev.* **2014**, 114, 10613−10653.

(13)   Pettiette-Hall, C. L.; Land, D. P.; McIver, R. T., Jr; Hemminger, J. C. Identification of Multiple Steps in the Dehydrogenation of Cyclic C6 Hydrocarbons to Benzene on Platinum(111). *J. Am. Chem. Soc.* **1991**, 113, 2755–2756.

(14)   Hansen, T. W.; Delariva, A. T.; Challa, S. R.; Datye, A. K. Sintering of Catalytic Nanoparticles: Particle Migration or Ostwald Ripening? *Acc. Chem. Res.* 2013, **46**, 1720−1730.

(15)   Iglesias-Juez, A.; Beale, A. M.; Maaijen, K.; Weng, T. C.; Glatzel, P.; Weckhuysen, B. M. A Combined In Situ Time-Resolved UV–Vis, Raman and High-Energy Resolution X-ray Absorption Spectroscopy Study on the Deactivation Behavior of Pt and PtSn Propane Dehydrogenation Catalysts Under Industrial Reaction Conditions. *J. Catal.* **2010**, 276, 268−279.

(16)   de Miguel, S. R.; Castro, A. A.; Scelza, O. A. FTIR and XPS Study of Supported PtSn Catalysts Used for Light Paraffins Dehydrogenation. *Catal. Lett.* **1996**, 36, 201−206.

(17)   Siri, G. J.; Ramallo-Lopez, J. M.; Casella, M. L.; Fierro, J. L. G.; Requejo, F. G.; Ferretti, O. A. XPS and EXAFS Study of Supported PtSn Catalysts Obtained by Surface Organometallic Chemistry on Metals:

Application to the Isobutane Dehydrogenation. *Appl. Catal., A* **2005**, 278, 239−249.

(18)   Shi, L.; Deng, G.-M.; Li, W.-C.; Miao, S.; Wang, Q.-N.; Zhang, W.-P.; Lu, A.-H. Al_2O_3 Nanosheets Rich in Pentacoordinate Al(3+) Ions Stabilize Pt-Sn Clusters for Propane Dehydrogenation. *Angew. Chem. Int.* Ed. **2015**, 54, 13994−1399.

(19)   Wang, G; Zhang, H.; Wang, H.; Zhu, Q.; Li, C.; Shan, H. The role of Metallic Sn Species in Catalytic Dehydrogenation of Propane: Active Component Rather than Only Promoter. *J. Catal.* **2016**, 344, 606−608.

(20)   Li, Q.; Sui, Z.; Zhou, X.; Zhu, Y.; Chen. D. Coke Formation on Pt–Sn/Al2O3 Catalyst in Propane Dehydrogenation: Coke Characterization and Kinetic Study. *Top. Catal.* **2011**, 54, 888−896.

(21)   Jablonski, E. L.; Castro, A. A.; Scelza, O. A.; de Miguel, S. R. Effect of Ga Addition to Pt/Al_2O_3 on the Activity, Selectivity and Deactivation in the Propane Dehydrogenation. *Appl. Catal. A* **1999**, 183, 189−198.

(22)   Redekop, E. A.; Galvita, V. V.; Poelman, H.; Bliznuk, V.; Detavernier, C.; Marin, G. B. Delivering a Modifying Element to Metal Nanoparticles via Support: Pt–Ga Alloying during the Reduction of Pt/Mg(Al,Ga)O_x Catalysts and Its Effects on Propane Dehydrogenation. *ACS Catal.* **2014**, 4, 1812−24.

(23)   Siddiqi, G.; Sun, P.; Galvita, V.; Bell, A. T. Catalyst Performance of Novel Pt/Mg(Ga)(Al)O Catalysts for Alkane Dehydrogenation. *J. Catal.* **2010**, 274, 200−206.

(24)   Sun, P.; Siddiqi, G.; Vining, W. C.; Chi, M.; Bell, A. T. Novel Pt/Mg(In)(Al)O Catalysts for Ethane and Propane Dehydrogenation. *J. Catal.* **2011**, 282, 165−174.

(25)   Dadras, J.; Jimenez-Izal, E., Alexandrova, A. N. Alloying Pt Sub-Nano-Clusters with Boron: Sintering Preventative and Coke Antagonist? *ACS Catal.* **2015**, 5, 5719−5727.

(26)   Ha, M.-A.; Baxter, E. T.; Cass, A. C.; Anderson, S. L.; Alexandrova, A. N. Boron Switch for Selectivity of Catalytic Dehydrogenation on Size-Selected Pt Clusters on Al_2O_3. *J. Am. Chem. Soc.* **2017**, 139, 11568−11575.

(27)   Perdew, J. P.; Burke, K.; Ernzerhof, M. Generalized Gradient Approximation Made Simple. *Phys. Rev. Lett.* **1996**, 77, 3865−3868.

(28)   Kresse, G.; Joubert, D. From Ultrasoft Pseudopotentials to the Projector Augmented-Wave Method. *Phys. Rev. B: Condens. Matter Mater. Phys.* **1999**, 59, 1758−1775.

(29)   Kresse, G.; Furthmüller, J. Efficiency of Ab-Initio Total Energy Calculations for Metals and Semiconductors Using a Plane-Wave Basis Set. *Comput. Mater. Sci.* **1996**, 6, 15–50.

(30)   Kresse, G.; Furthmüller, J. Efficient Iterative Schemes for *Ab Initio* Total-Energy Calculations Using a Plane-Wave Basis Set. *Phys. Rev. B: Condens. Matter Mater. Phys.* **1996**, 54, 11169-11186.

(31)   Kresse, G.; Hafner, J. *Ab Initio* Molecular Dynamics for Liquid Metals. Phys. Rev. B: Condens. *Matter Mater. Phys.* **1993**, 47, 558−561.

(32)   Kresse, G.; Hafner, J. *Ab Initio* Molecular-Dynamics Simulation of the Liquid-Metal–Amorphous-Semiconductor Transition in Germanium. Phys. Rev. B: Condens. *Matter Mater. Phys.* **1994**, 49, 14251−14269.

(33)   Wales, D. J.; Doye, J. P. Global Optimization by Basin-Hopping and the Lowest Energy Structures of Lennard-Jones Clusters Containing up to 110 Atoms. *J. Phys. Chem. A* **1997**, 101, 5111−5116.

(34)   Zhai, H.; Alexandrova, A. N. Ensemble-Average Representation of Pt Clusters in Conditions of Catalysis Accessed through GPU Accelerated Deep Neural Network Fitting Global Optimization. *J. Chem. Theor. Comput.* **2016**, 12, 6213−6226.

(35)   Giannozzi, P.; Baroni, S.; Bonini, N.; Calandra, M.; Car, R.; Cavazzoni, C.; Ceresoli, D.; Chiarotti, G. L.; Cococcioni, M.; Dabo, I.; Dal Corso, A.; Fabris, S.; Fratesi, G.; de Gironcoli, S.; Gebauer, R.;

Gerstmann, U.; Gougoussis, C.; Kokalj, A.; Lazzeri, M.; Martin-Samos, L.; Marzari, N.; Mauri, F.; Mazzarello, R.; Paolini, S.; Pasquarello, A.; Paulatto, L.; Sbraccia, C.; Scandolo, S.; Sclauzero, G.; Seitsonen, A. P.; Smogunov, A.; Umari, P.; Wentzcovitch, R. M. QUANTUM ESPRESSO: A Modular and Open-Source Software Project for Quantum Simulations of Materials. *J. Phys. Condens. Matter* **2009**, 21, 395502–395521.

(36)   Argyle, M. D.; Bartholomew, C. H. Heterogeneous Catalyst Deactivation and Regeneration: A Review. *Catalysts* **2015**, 5, 145−269.

(37)   Augusto, C. C. C.; Zotin, J. L.; da Costa Faro, A. Effect of Sulfur or Nitrogen Poisoning on the Activity and Selectivity of Y-Zeolite-Supported Pt–Pd Catalysts in the Hydrogenation of Tetralin. *Cat. Lett.* **2001**, 75, 37−43.

(38)   Yang, F.; Chen, M. S.; Goodman, D. W. Sintering of Au Particles Supported on TiO_2(110) during CO Oxidation. *J. Phys. Chem. C* **2009**, 113, 254–260.

(39)   Kang, S. B.; Lim, J. B.; Jo, D.; Cho, B. K.; Hong, S. B.; Kim, C. H.; Oh, S. H. Ostwald-Ripening Sintering Kinetics of Pd-based Three-Way Catalyst: Importance of Initial Particle Size of Pd. *Chem. Eng. J.* **2017**, 316, 631–644.

(40)   Campbel, C. T. The Effect of Size-Dependent Nanoparticle Energetics on Catalyst Sintering. *Acc. Chem. Res.* **2013**, 46, 1712–1719.

(41)   Shaikhutdinov, S. K.; Frank, M.; Bäumer, M.; Jackson, S. D.; Oldman, R. J.; Hemminger, J. C.; Freund, H. Effect of Carbon Deposits on Reactivity of Supported Pd Model Catalysts. *Catal. Lett.* **2002**, 80, 115–122.

(42)   Neurock, M.; van Santen, R. A. A First Principles Analysis of C−H Bond Formation in Ethylene Hydrogenation. *J. Phys. Chem. B* **2000**, 104, 11127–11145.

(43)   Chen, Y.; Vlachos, D. G. Hydrogenation of Ethylene and Dehydrogenation and Hydrogenolysis of Ethane on Pt(111) and Pt(211): A Density Functional Theory Study. *J. Phys. Chem. C* **2010**, 114, 4973–4982.

(44)   Anderson, A. B.; Choe, S. Ethylene Hydrogenation Mechanism on the Platinum(111) Surface: Theoretical Determination. *J. Phys. Chem.* **1989**, 93, 6145– 6149.

(45)   Shin, E. W.; Kang, J. H.; Kim, W. J.; Park, J. D.; Moon, S. H. Performance of Si-modified Pd Catalyst in Acetylene Hydrogenation: the Origin of the Ethylene Selectivity Improvement. *Appl. Cat. A: Gen.* **2002**, 223, 161–172.

(46)   Kim, W. J.; Shin, E. W.; Kang, J. H.; Moon, S. H. Performance of Si-modified Pd Catalyst in Acetylene Hydrogenation: Catalyst Deactivation Behavior. *Appl. Cat. A: Gen.* **2003**, 251, 305–313.

(47)   Kim, W. J.; Moon, S. H. Modified Pd Catalysts for the Selective Hydrogenation of Acetylene. *Cat. Today* **2012**, 185, 2–16.

(48)   Shen, L.; Dadras, J.; Alexandrova, A. N. Pure and Zn-Doped Pt Clusters Go Flat and Upright on MgO(100). *Phys. Chem. Chem. Phys.* **2014**, 16, 264366–26442.

(49)   Baxter, E. T.; Ha, M.-A.; Cass, A. C.; Zhai, H.; Alexandrova, A. N.; Anderson, S. L. Diborane Interactions with Pt_7/Alumina: Preparation of Size-Controlled Borated Pt Model Catalysts. *J. Phys. Chem. C* **2018**, 122, 1631-1644.

(50)   Yoon, B.; Häkinnen, H.; Landman, U.; Wörz, A. S.; Antonietti, J.-M.; Abbet, S.; Judai, K.; Heiz, U. Charging Effects on Bonding and Catalyzed Oxidation of CO on Au_8 Clusters on MgO. *Science* **2005**, 307, 403-407.

TOC Graphics: